Published in final edited form as:
J Immunol. 2008 August 15; 181(4): 2465–2471.

Lymphocyte Electrotaxis in vitro and in vivo

Francis Lin[*,†,¶,§], **Fabio Baldessari**[‡,§], **Christina Crenguta Gyenge**[*,†], **Tohru Sato**[*,†], **Robert D. Chambers**[‡], **Juan G. Santiago**[‡], and **Eugene C. Butcher**[*,†,¶]

* *Laboratory of Immunology and Vascular Biology, Department of Pathology, School of Medicine, Stanford University, Stanford, California, 94305, USA*

† *Center for Molecular Biology and Medicine, Veterans Affairs Palo Alto Health Care System, Palo Alto, California, 94304, USA*

‡ *Department of Mechanical Engineering, Stanford University, Stanford, California, 94305, USA*

Abstract

Electric fields are generated in vivo in a variety of physiologic and pathologic settings, including penetrating injury to epithelial barriers. An applied electric field with strength within the physiologic range can induce directional cell migration (i.e. electrotaxis) of epithelial cells, endothelial cells, fibroblasts, and neutrophils suggesting a potential role in cell positioning during wound healing. In the present study, we investigated the ability of lymphocytes to respond to applied direct current (DC) electric fields. Using a modified transwell assay and a simple microfluidic device, we show that human peripheral blood lymphocytes migrate toward the cathode in physiologically relevant DC electric fields. Additionally, electrical stimulation activates intracellular kinase signaling pathways shared with chemotactic stimuli. Finally, video microscopic tracing of GFP-tagged immunocytes in the skin of mouse ears reveals that motile cutaneous T cells actively migrate toward the cathode of an applied DC electric field. Lymphocyte positioning within tissues can thus be manipulated by externally applied electric fields, and may be influenced by endogenous electrical potential gradients as well.

Keywords

T cells; Cell Trafficking; Transgenic/Knockout Mice

Introduction

Directed cell migration is essential to numerous physiological processes including immune responses, wound healing, cancer metastasis and neuron guidance (1–3). Chemotaxis and haptotaxis, directed migration in response to soluble or surface bound chemoattractant gradients, have been well characterized. In addition to chemical signals, an electric field can

¶Corresponding Authors Laboratory of Immunology and Vascular Biology, Department of Pathology, School of Medicine, Stanford University, Stanford, California 94305, USA., Tel: (650) 852-3369, Fax: (650) 858-3986, E-mail: flin2@stanford.edu for F. Lin, ebutcher@stanford.edu for E.C. Butcher.
§These authors contributed equally to this work

Disclosures: The authors have no financial conflict of interest.

be generated in vitro and in vivo, and such fields can also direct cell movement in a process called electrotaxis or galvanotaxis (4–6). In-vitro studies have demonstrated electrotaxis of a number of different cell types in response to direct current (DC) electric fields of a magnitude experienced in vivo (e.g. in healing wounds) (4–6). Some cells migrate towards the cathode (e.g. neural crest cells, fibroblasts, keratinocytes, rat prostate cancer cells, mouse neutrophils, human myeloid cell lines, and many epithelial cell types)(7–16), and others migrate to the anode (e.g. corneal endothelial cells, and human vascular endothelial cells)(17–19). Such electrotactic mechanisms have the potential to contribute to cellular positioning in multiple physiologic settings (4–6). As one example, disruption of epithelial integrity leads to an electric field oriented toward the wound (~0.4V/cm–1.4V/cm); surrounding epithelial cells migrate directionally to cover the wounded tissue in a process that can be disrupted by interfering with the electric fields (4,16).

Here we have investigated the effects of applied electric fields on the migration of human peripheral blood lymphocytes. We evaluated T cell responses to electric fields by direct monitoring of migration both in vitro in a controlled chamber environment, and in vivo in mouse skin. Our results show that all circulating lymphocyte classes display electrotaxis to applied electric fields, that the electrotaxis of T cells can be at least as directionally efficient as reported chemotactic responses, and that electric fields can control T cell movement in vivo.

Materials and Methods

Cell Preparation

Human buffy coats were obtained from healthy blood donors (Stanford Blood Center). Human peripheral blood mononuclear cells (hPBMC) were isolated from the buffy coat using standard gradient centrifugation. Memory T cells (CD45RA-CD45RO+ T cells) from hPBMC were negatively selected by MACS (magnetic cell separation, Miltenyi Biotec Inc., CA). hPBMC and purified memory T cells were re-suspended in supplemented culture medium (RPMI-1640 GLUTAMAX medium with 25mM HEPES buffer (Gibco, CA), 1% Penicillin-Streptomycin and 10% heat-inactivated FBS). The cells were kept in a 37°C incubator with 8% CO_2 injection and were used for experiment within 48 hours after separation.

Transwell Assay

Cell migration in an applied electric field was tested using transwell assays (COSTAR 24-well plate with inserts, 5μm pore, Corning, NY). Briefly, migration medium, consisting of RPMI-1640 with 10% FBS and 10^6 hPBMC in a 100μL volume, was added to the top well, and medium alone was added to the bottom well in a 600μL volume. An electric field was applied to the transwell (2.5V across the transwell) by placing two platinum electrodes, which were connected to a DC power supply, to the top and bottom well of the transwell (Fig. 1A). The electrical potential in the transwell assay was simulated using COMSOL Multiphysics 3.3a (Comsol, Palo Alto, CA)(Fig. 1)(20). The current was measured to be stable for at least 1.5 hours. Cells were allowed to migrate from the top well to the bottom well through the filter. The migration of cells in DC electric field was assayed for 1.5 hours in a 37°C incubator. Then, the inserts were removed, and the cells that had migrated through the filter to the bottom well were transferred to a FACS tube for staining of different cell markers. Antibodies against human CD3 (BD Biosciences, CA), CD4 (BD Biosciences, CA), CD8 (eBioscience, CA) CD45RA (BD Biosciences, CA), CD45RO (Biolegend, CA), CD19 (BD Biosciences, CA) and CD56 (BD Biosciences, CA) were used following the manufacturer's recommendation. The stained cell samples were mixed with calibration beads (10,000 beads in 50μL, Polysciences, Inc., PA) and were analyzed using a flow cytometer (LSR-II systems, BD Biosciences, CA). The FACS data were further analyzed using FlowJo (Tree Star, Inc., OR). The percentage of migrated cells of each cell type was calculated. The same experiment was repeated with

reversed DC electric field or without the field for comparison. Each experimental condition was repeated multiple times (n = 9~11). The average and the standard error of the mean (s.e.m) were calculated for each condition, and the Student's *t*-test was performed for comparison ($p < 0.05$). Note that the range of potentials that can be evaluated in this system is limited: Current values observably fluctuated at lower fields (presumably due to operating near the sub-ohmic regime). Higher fields were difficult in our setup due to the generation of electrolysis bubbles.

Preparation of Microfluidic Device

The microfluidic device was fabricated in optically clear plastic, which contains laser-cut microchannels (Fig. 3). Briefly, each microfluidic device consists of a microscope glass slide (75 × 25 × 1mm, VWR), one 100 μm thick Melinex sheet with adhesive on both sides (Fralock Division of Lockwood Ind. Inc., San Carlos, CA), one 50 μm thick Melinex sheet with no adhesive (Fralock Division of Lockwood Ind. Inc., San Carlos, CA), and two 200 μL pipette tips. The glass slide constitutes the bottom of the microfluidic device. The 100μm thick Melinex sheet constitutes the side walls of the microchannel. For rapid prototyping, we used a CO_2 laser cutter (Universal Laser Systems, Scottsdale, AZ) to machine the intended channel shape in this sheet. Each channel was approximately 1.5cm in length, 500μm in width, and 100μm in depth. For the wells, we cut 1.5mm diameter holes at both ends of the channel. Similarly, we cut 1.5mm diameter holes in the 50 μm thick Melinex sheet. The 50μm thick sheet was used to seal the top of the channel, and the holes were cut in correspondence to the wells of the channel. We designed the channel layout using the software AutoCAD (AutoDESK, San Rafael, CA). For assembly, the double-adhesive Melinex sheet was potted onto the pre-cleaned glass slide. The microchannel was sealed using the 50μm thick sheet, aligning the holes with the channel wells. Finally, two 200μL pipette-tips were cut to remove the sharp tips and were each aligned with one hole, and potted with epoxy (Devcon, MA) to serve as medium reservoirs. Before use, the channel was coated with fibronectin (Fisher) for 2 hours at room temperature, providing a substrate for cell adhesion and migration. A new device was used for each experiment.

Cell Migration Experiment in Microfluidic Device

For each experiment, a few thousand cells were loaded into the microfluidic device from the wells and allowed to settle in the fibronectin-coated channel for ~10min in a 37°C incubator. Then, approximately 150μL medium (RPMI-1640 with 10% FBS) were added to each reservoir. Two platinum electrodes (0.25mm diameter, Omega, CT) connecting to a DC power supply (Agilent Technologies, CO) were placed in the medium reservoirs to complete the circuit. The device was placed on a microscope stage (Axiovert 35, Carl Zeiss, Inc., Germany) and the system was allowed to equilibrate for ~5 min (wait until no flowing cells were seen in the channel). Then, the DC electric field was applied, and cell migration (in a selected ~550μm(W) × 800μm(L) microscope field using a 10× objective) was recorded by time-lapse microscopy at 6 frames min^{-1} for 30min to 2 hours at room temperature using a solid state camera (Model No. 4815-2000, Cohu, Inc., CA). The image acquisition was controlled by VCE Pro (1st. Vision, Inc., CA).

Cell Tracking and Data Analysis

Movement of individual cells was tracked using ImageJ (v1.34s, NIH, MD)(21). Background of the images was subtracted and the noise was removed using the "despeckle" function. Then the images were calibrated to distance. Only the cells that migrated within the microscope field were selected and tracked using the "Manual Tracking" plug-in in ImageJ. The tracking data were exported to Excel and Oriana for analysis. Over 100 cell tracks from multiple independent experiments were analyzed.

The movement of cells was quantitatively evaluated by (1) percentage of cells migrated toward the cathode of the electric field (%); (2) electrotactic index (E.I.), which is the ratio of the

displacement of cells toward the cathode of the electric field (Δy) to the total migration distance (d): $E.I. = \Delta y/d$; (3) the average speed: $V = d/\Delta t$; *E.I.* and *V* were presented as the average value plus/minus the standard error of the mean (s.e.m.) of all cells: average ± s.e.m.; (4) statistical analysis of migration angles was performed using Oriana for Windows (Kovach Computing Services, Wales, UK) to examine the directionality of the cell movement. Specifically, migration angles (calculated from x-y coordinates at the beginning and the end of the cell tracks) were summarized in a direction plot, which is a rose diagram showing the distribution of angles grouped in 20° intervals, with the radius of each wedge indicating cell number. The Rayleigh test for circular uniformity was applied, with a significance level of 0.05. When there was significant directionality, the mean angle and the 95% confidence interval were calculated. A Modified Rayleigh test (V test) was also applied, in order to test whether deviations from the direction of electric field (90° or 270°) were significant.

Phospho-Flow Cytometry

Human peripheral blood lymphocytes (3.5×10^6) resuspended in 500μL RPMI-1640 medium were stimulated in a 24-well plate by an applied electric field (2.5V across ~1.3cm for 60min at room temperature; Two platinum electrodes connecting to a DC power supply were placed in the cell-containing medium to generate the electric field). Stimulated cells were immediately fixed in 2% paraformaldehyde (2% PFA in PBS) for 10 min at room temperature and then permeabilized in 100% methanol at −20°C overnight. Control cells were treated similarly but without exposure to the electric field. Cells were then washed twice with staining buffer (0.5% BSA in PBS) and stained with Alexa Fluor 488-conjugated phospho-Erk1/2 (T202/Y204) or Alexa Fluor 647-conjugated phospho-Akt-ser473 antibody (BD Biosciences, CA). Cells were analyzed using a flow cytometer (LSR-II systems, BD Biosciences, CA). The FACS data were further analyzed using FlowJo (Tree Star, Inc., OR).

Confocal Microscopy of Cell Migration in Mouse Ear Tissue

Transgenic mice heterozygous for *Cxcr6* (*Cxcr6gfp/+*), B6.129P2-*Cxcr6tm1Litt/J* crossed with C57BL/6J (The Jackson Laboratory, Bar Harbor, ME) were used. These mice have one *Cxcr6* allele replaced by enhanced green fluorescent protein (GFP) marking activated and memory CD4 and CD8 T cells fluorescent green, which can be visualized by fluorescent microscopy and flow cytometry (22). The in-vivo imaging experiments were performed under an approved animal use protocol. For each experiment, a *Cxcr6gfp/+* mouse was anesthetized by inhaled isoflurane (Table top lab animal anesthesia system, VetEquip, Inc., CA) followed by ketamine/xylazine anesthesia. Under anesthesia, two platinum electrodes (0.25mm diameter, Omega, CT) connecting to a DC power supply (Agilent Technologies, CO) were surgically inserted to the peripheral tissue of the mouse ear, approximately 5mm apart. Then the mouse was placed on the stage of a confocal microscope (LSM 510 META, Carl Zeiss, Inc., Germany), and the ear was pressed onto a glass coverslide, which was mounted on the slide holder. The rest of the mouse body was electrically isolated from the microscope stage. The GFP^+ cells in the mouse ear was imaged (Ar laser, 488nm wavelength) with or without the externally applied DC electric field (1V–2.5V across ~5mm) for 1~2 hours at about 80 sec per scanning cycle using a 10× or a 20× objective. For each scanning cycle, 20 images at 5μm intervals along the Z direction were captured. The “stack” of images associated with each scanning cycle was then depth-averaged and processed in MATLAB (MathWorks, Natick, MA). Using the DIPimage MATLAB package (Quantitative Imaging Group, Delft, NL), we aligned, background-subtracted, and conditioned each frame to remove stationary features. We then tracked the moving cells with a particle tracking velocimetry algorithm (D. Blair and E. Dufresne, http://physics.georgetown.edu/matlab/). Briefly, the algorithm located cells’ centroids with subpixel accuracy and tracked cells between frames using a chi-squared minimization process based on cell displacement, constrained by a maximum cell velocity. To reduce noise, we ignored cells which were tracked for fewer than five frames, or which were

not sufficiently displaced (less than 2 cell diameters). We chose threshold parameters, which maximized the number of tracked cells without causing discernible false positives. The tracking data was further analyzed to calculate the displacement of each cell in the X and Y direction, and the electrotactic index.

Results

Electrotactic response of human peripheral blood lymphocytes and monocytes in transwell assays

We applied the transwell assay, a conventional method for studies of leukocyte chemotaxis, to determine whether blood mononuclear cells would respond to an applied electric field. Platinum electrodes were arranged in the top and bottom wells to allow application of an electric field (see materials and methods)(Fig. 1A). Numerical simulations using specialized modeling software COMSOL Multiphysics 3.3a (Comsol, Palo Alto, CA) were used to model the configuration: the simulation indicates that application of 2.5V across the transwell yields an electrical potential gradient along the vertical direction in the top well that is close to the physiologic range seen in wounds (Fig. 1). Human peripheral blood mononuclear cells (hPBMC) were added to the top well and allowed to migrate in the presence or absence of the applied field. Immunofluorescence staining and cytometric analysis of input and migrated cell populations allowed assessment of the efficiency of migration of each of the hPBMC subsets indicated (Fig. 2).

Compared to spontaneous migration in the absence of a field, there was a significant increase in migration of all lymphocyte subsets except NK cells when the cathode was in the lower well. Moreover, the magnitude of the effect was similar for CD4 T cells, CD8 T cells, naive T cells, memory T cells, B cells, and for monocytes. In contrast, migration was not enhanced when the field was applied in the opposite orientation, indicating that the migration is directional. Compared to other blood lymphocytes, NK cells displayed high background migration (a well known characteristic of these cells), potentially obscuring any electrotaxis. Moreover, when the field was reversed NK cell migration to the bottom well was suppressed below background, supporting an electrotactic response to the cathode in the upper well (Fig. 2). Thus, these results support the hypothesis that human blood lymphocytes and monocytes undergo cathode-directed electrotaxis, and that in contrast to chemotactic receptor driven responses, which are characteristically subset-selective, the electrotactic response is remarkably uniform among the major lymphocyte classes.

Electrotaxis of memory T cells in a microfluidic visualization chamber

To confirm and visualize the lymphocyte electrotactic response and evaluate the efficiency of orientation of migrating cells towards the cathode in controlled electric fields, we traced the migration of purified memory T cells from human PBMC migrating on a fibronectin-coated coverslide (see materials and methods)(Fig. 3). A synthesized channel and medium reservoirs were filled with migration medium, cells were added and allowed to adhere, and the electric field was applied using platinum electrodes in the two medium reservoirs. The migratory behavior of cells in the channel was recorded by video microscopy. Compared with the transwell assay, the microfluidic device can generate a well-defined uniform electric field in the microchannel, and allows visualization and quantitative assessment of cell migration.

We applied an electric field of 1V cm^{-1}, similar to fields observed in wound tissue (16). The field induced a current on the order of 2 μA, which was stable over the 1.5 hour period. Almost all adherent T cells migrated, and a high percentage migrated toward the cathode of the applied electric field (Fig. 4C). The electrotactic index (mathematically analogous to the widely used chemotactic index (21,23–25)) is presented (Fig. 4C). Statistical analysis of migration angles

shows that the distribution of migration angles is highly correlated with the direction of the applied electric field (Fig. 4B). The quantitative analysis also agrees with direct visualization of cell tracks (Fig. 4A). In addition, the cells exhibited a relatively high migration speed in electric field (Fig. 4C), comparable to the optimal speed of T cells we observed in response to chemoattractant stimuli (21). No significant movement of cells was detected in the absence of an applied electric field: cells in this model are adherent and non-motile in the absence of a chemoattractant or electric field (data not shown). When the electric field was inverted, the cells reversed direction and now migrated toward the new cathode (Fig. 4D–F). We conclude that T cell migration can be directed by physiologically-relevant applied electric fields in vitro. The efficiency of migration (the electrotactic index) is slightly higher than the chemotactic index we observed in a similar study tracing T cell chemotaxis (21), and higher than the optimal chemotactic index we observed in earlier studies of neutrophil chemotaxis in under agarose assays (26,27) and a 3D fibrin gel assay (25).

Electric fields induce T cell signaling responses

Directional migration of cells is orchestrated by a cascade of intracellular signaling events that coordinate actin polymerization, membrane and cellular polarization, protrusion and adhesion mechanisms (28). Well-characterized intracellular responses to chemoattractants include activation of kinase cascades such as phosphorylation of Erk1/2 (a member of MAP Kinase family) (29) and Akt (a downstream signaling molecule of PI3 Kinase pathway). Kinase responses have also been associated with electrotaxis of neutrophils (16). To confirm triggering of intracellular signals in T cells, we applied an electric field and measured its effects on Erk1/2 and Akt in human peripheral blood lymphocytes using flow cytometric methods (see materials and methods).

As shown in Fig 5, Erk1/2 and Akt phosphorylation were increased in cells exposed for 60 minutes to an electric field, confirming the engagement of intracellular kinase cascades. Shorter electrical stimulation (i.e. 1min or 10min) did not induce detectable increases of Erk1/2 or Akt phosphorylation (data not shown). Thus, intracellular signaling events shared with chemotactic responses are triggered in lymphocytes activated by an electric field.

T cell electrotaxis in vivo

As mentioned above, epithelial injury induces an electric field oriented toward the wound and similar in magnitude to that used in our experiments (16), suggesting a potential role for electrotaxis in recruitment of regulatory or memory T cells and other leukocytes from surrounding tissue. Analyzing leukocyte electrotaxis in response to physiologic electric field produced by a wound, however, is complicated by the fact that tissue injury releases multiple chemoattractants, to which subsets of T cells also respond. We therefore asked whether an externally applied electric field can direct migration of lymphocytes in vivo in a homeostatic setting, in which inflammatory chemotactic mechanisms can be distinguished from electric-field-induced cellular responses. We took advantage of genetically modified mice which express green fluorescent protein (GFP) under the promoter of the chemokine receptor CXCR6 (30). In these mice, GFP is highly expressed in subsets of tissue lymphocytes, allowing their movement to be followed by time-lapse confocal microscopy. Imaging in the living ear reveals scattered small GFP+ cells, with morphological characteristics consistent with polarized migrating lymphocytes (Fig. 6A, circled cells). Most of these small GFP+ cells were spontaneously motile (Fig. 6B). Consistent with expression of CXCR6 by γδT cells (31), flow cytometric analysis reveals that among cells rendered efficiently into suspension (a process which enriches lymphocytes), most lymphocytic cells isolated from ear skin are CD3+ (76% of GFP+ cells), and many express γδTCR (56% of total GFP+ cells). A more abundant GFP+ population, consisting of larger cells with dendritic morphology, is also present in the ear skin; these cells are prominent in confocal fluorescence imaging (Fig. 6A; not circled cells) and were

sessile over the periods of observation studied, whether or not an external electric field was applied.

In the absence of an applied electric field (with electrodes inserted into the ear but without voltage), the lymphocytic GFP cells migrated randomly (Fig. 6B, Video 1). When an electric field was applied (1V–2.5V across ~5mm in the peripheral ear tissue), however, these GFP cells preferentially migrated toward the cathode within the microscope field. The negative electrode was located approximately 2mm from the microscope field. Individual cells migrated as much as 100 μm towards the cathode over the 1~2 hrs period of experiment (Fig. 6C, Video 2). It is worth pointing out that the images were depth averaged and projected onto a common 2D plane for tracking analysis. However, some cells moved outside of the visible field in the Z direction and were lost from analysis during the observation period. Therefore the mean distance of cell migration visualized was less than the actual migration distance in 3D tissues; The velocity of migration of motile cells was similar in the presence or absence of the applied field (i.e. 0.34 ± 0.02 μm/min (average ± s.e.m.) in the absence of the field versus 0.43 ± 0.04 μm/min (average ± s.e.m.) in the applied field. $p = 0.17$). We conclude that lymphocytes can be directed in vivo by externally applied electric fields.

Discussion

Our studies show that normal blood lymphocytes and monocytes respond to a steady electric field in transwell assays. All lymphocyte subsets examined, including naïve and memory CD4, CD8 T cells, and B cells migrated towards the cathode, as did monocytes. Electrotactic migration is highly directional: that in studies monitoring the migratory path of memory T cells on fibronectin-coated glass, almost all cells migrated cathodally, and the directionality index is comparable to or higher than the optimal directionality index observed in comparable chemotaxis assays. We also confirm that electric field exposure induces Erk1/2 and Akt activation in T cells, consistent with activation of the MAP Kinase and PI3 Kinase signaling pathways implicated in coordinated cell motility. Finally, we show that an applied electric field induced the electrotactic migration of endogenous lymphocytes in mouse skin. Our results thus define electrotaxis as potentially an additional mechanism for the control of lymphocyte and monocyte migration.

Electrotaxis of eukaryotic cells has been reported in a number of studies (4,6). Particularly, electrotaxis of epithelial cells plays an important role in controlling wound healing (i.e. the wound generates an inward DC electric field and electrotaxis of epithelial cells toward the cathode of the electric field helps closing the wound) (4,16). Our results show that memory T cells migrate toward the cathode of an electric field applied with strength similar to wound generated electric field. Therefore, electrotaxis of lymphocytes and other immune cells may be involved in the process of wound healing as well. Furthermore, our study shows that immune cell positioning can be regulated in vivo by externally applied electric fields.

An interesting aspect of our results is the uniformity in the electrotactic responses of different mononuclear leukocyte subsets as assessed in the transwell assay. This contrasts with responses to known chemoattractants, whose cell surface receptors are differentially expressed and direct subset-selective migration. The uniform migration of circulating lymphocytes suggests that other leukocyte subsets (e.g. tissue memory cells) may undergo electrotaxis as well. On the other hand, not all GFP+ cells in mouse skin responded: rather the electrotactic responses appeared limited to cells that were intrinsically motile, i.e. cells that displayed random migration prior to field application. Thus, leukocyte responses to electric potential gradients may be regulated primarily by the migratory state of competence of the cells, rather than (as in the case of chemotactic response) by subset specificity among migratory populations.

Indeed, as suggested by the diverse cell types that respond, from Dictyostelium amoebae to epithelial cells, metastatic cancer cells and lymphocytes, electrotaxis may be a nearly universal competency of motile cells (4,6). Regulation of electrotaxis may be possible in terms of directionality, however. Although lymphocytes, like many other mammalian cells, undergo cathode-directed electrotaxis, some cells (e.g. corneal endothelial cells, human vascular endothelial cells) migrate preferentially to the anode. Given the absence of subset selectivity in lymphocyte responses, however, it seems unlikely that electric fields operate in vivo to control the recruitment of lymphocytes from the blood or direct their microenvironmental interactions during physiologic immune responses. Instead, physiologic electric fields may serve to support cellular translocation events in settings where cell type specificity is not a critical issue. One example would be the bulk cell population movements that occur early in embryogenesis, when the principal distinction is between motile and non-motile undifferentiated cells; indeed the role of electric fields in cell movement was implicated in studies of early embryogenesis (4,5). A more pertinent example is the cellular response to a penetrating wound, during which the rapid recruitment of any motile cell (fibroblasts, macrophages and other immune cells) from the immediately surrounding tissue would seem beneficial or at least not deleterious. As mentioned in the introduction, epithelial surfaces such as the skin are well documented batteries, maintaining an electrical potential gradient that is short circuited upon disruption of the epithelial barrier. Wounds in bovine cornea or in guinea pig and human skin, for example, generate local electric fields of ~0.4–1.4V cm^{-1} with the wound itself being the cathode. This field is well within the range for efficient electrotactic recruitment of lymphocytes and other motile cells into the wound. While in the case of lymphocytes and other immune cells it may be difficult in such a setting to isolate the effects of electrotaxis from those of the chemoattractants induced, our studies clearly show that lymphocytic cells resident in skin respond with directional migration when presented with an applied electric field.

Previous studies have found that electric fields activate intracellular signaling processes including kinase pathways involved in cellular motility. We have confirmed here that lymphocytes respond to electric fields with activation of Erk kinases and Akt, which are involved in chemoattractant receptor signaling and in electrotactic signaling in other cells (16,29,32). Activation of these pathways suggests that electrotaxis and chemotaxis engage common intracellular cell motility programs in responding lymphocytes. On the other hand, in keeping with findings in Dictyostelium amoebae in which electric fields did not generate a rapid burst of calcium signaling (but only a slow, prolonged calcium response at the population level), (32), we did not observe a robust, immediate calcium flux in lymphocytes in response to electrical stimulation, and delayed calcium elevation assessed by flow cytometric analysis of Fluo-4 labeled cells was variable (data not shown). The kinetics of MAP kinase and Akt signaling also distinguishes the electric field response, since phosphorylation of Erk and Akt was significant after 60 minutes, but was not appreciable by phospho-flow analyses at 1 or 10 minutes, contrasting with the rapid triggering of signaling cascades by chemoattractant receptors. In conclusion, our study demonstrates electrotaxis of lymphocytes, and shows that electric fields can direct lymphocyte migration in vitro and in vivo. Electrotaxis represents an additional mechanism for the control of leukocyte migration. It is likely to play a role in sites of epithelial injury, and may permit novel approaches for manipulating the positioning of lymphocytes and other immunocytes to enhance vaccine or anti-tumor responses.

Supplementary Material

Refer to Web version on PubMed Central for supplementary material.

Acknowledgements

We thank The Stanford Blood Center for technical support. We thank Tarun Khurana for helping with the fabrication of microfluidic devices; Dr. Hekla Sigmundsdottir and Lusijah Rott for helping with flow cytometry.

Grant Support:

F. L. is supported by the postdoctoral training grant (5T32AI07290-20) from the NIH-NIAID, Immunology Program, Stanford University, and a grant from the Stanford Bio-X Interdisciplinary Initiative Program. F. B. is supported by a grant from the Stanford Bio-X Interdisciplinary Initiative Program. T.S. is supported by the grant R03DK069395. This study is supported by a grant from the Stanford Bio-X Interdisciplinary Initiative Program to E.C.B., J.G.S. and F.L., and in part by grants from the NIH to E.C.B. and J.G.S., and an award from the Department of Veterans Affairs to E.C.B..

Abbreviation

DC
direct current

EF
electric field

FACS
fluorescent-activated cell sorting

GFP
green fluorescent protein

hPBMC
human peripheral blood mononuclear cells

References

1. Condeelis J, Jones J, Segall J. Chemotaxis of metastatic tumor cells: clues to mechanisms from the Dictyostelium paradigm. Cancer Metastasis Rev 1992;11:55–68. [PubMed: 1511497]
2. Kubes P. Introduction: The complexities of leukocyte recruitment. Seminars in Immunology 2002;14:65–72. [PubMed: 11978078]
3. Song H, Poo M. Signal transduction underlying growth cone guidance by diffusible factors. Curr Opin Neurobiol 1999;9:355–363. [PubMed: 10395576]
4. McCaig CD, Rajnicek AM, Song B, Zhao M. Controlling Cell Behavior Electrically: Current Views and Future Potential. Physiol Rev 2005;85:943–978. [PubMed: 15987799]
5. Robinson KR, Messerli MA. Left/right, up/down: the role of endogenous electrical fields as directional signals in development, repair and invasion. BioEssays 2003;25:759–766. [PubMed: 12879446]
6. Mycielska ME, Djamgoz MB. Cellular mechanisms of direct-current electric field effects: galvanotaxis and metastatic disease. J Cell Sci 2004;117:1631–1639. [PubMed: 15075225]
7. Cooper MS, Keller RE. Perpendicular orientation and directional migration of amphibian neural crest cells in dc electrical fields. Proc Natl Acad Sci U S A 1984;81:160–164. [PubMed: 6582473]
8. Sheridan DM, Isseroff RR, Nuccitelli R. Imposition of a physiologic DC electric field alters the migratory response of human keratinocytes on extracellular matrix molecules. J Invest Dermatol 1996;106:642–646. [PubMed: 8617998]
9. Onuma EK, Hui SW. A calcium requirement for electric field-induced cell shape changes and preferential orientation. Cell Calcium 1985;6:281–292. [PubMed: 3926320]
10. Djamgoz MBA, Mycielska M, Madeja Z, Fraser SP, Korohoda W. Directional movement of rat prostate cancer cells in direct-current electric field: involvement of voltagegated Na+ channel activity. J Cell Sci 2001;114:2697–2705. [PubMed: 11683396]

11. Zhao M, Dick A, Forrester JV, McCaig CD. Electric field-directed cell motility involves up-regulated expression and asymmetric redistribution of the epidermal growth factor receptors and is enhanced by fibronectin and laminin. Mol Biol Cell 1999;10:1259–1276. [PubMed: 10198071]
12. Zhao M, McCaig CD, Agius-Fernandez A, Forrester JV, Araki-Sasaki K. Human corneal epithelial cells reorient and migrate cathodally in a small applied electric field. Curr Eye Res 1997;16:973–984. [PubMed: 9330848]
13. Zhao M, Agius-Fernandez A, Forrester JV, McCaig CD. Directed migration of corneal epithelial sheets in physiological electric fields. Invest Ophthalmol Vis Sci 1996;37:2548–2558. [PubMed: 8977469]
14. Zhao M, Agius-Fernandez A, Forrester JV, McCaig CD. Orientation and directed migration of cultured corneal epithelial cells in small electric fields are serum dependent. J Cell Sci 1996;109(Pt 6):1405–1414. [PubMed: 8799828]
15. Li X, Kolega J. Effects of direct current electric fields on cell migration and actin filament distribution in bovine vascular endothelial cells. J Vasc Res 2002;39:391–404. [PubMed: 12297702]
16. Zhao M, Song B, Pu J, Wada T, Reid B, Tai G, Wang F, Guo A, Walczysko P, Gu Y, Sasaki T, Suzuki A, Forrester JV, Bourne HR, Devreotes PN, McCaig CD, Penninger JM. Electrical signals control wound healing through phosphatidylinositol-3-OH kinase-gamma and PTEN. Nature 2006;442:457–460. [PubMed: 16871217]
17. Rapp B, de Boisfleury-Chevance A, Gruler H. Galvanotaxis of human granulocytes. Dose-response curve. Eur Biophys J 1988;16:313–319. [PubMed: 3240758]
18. Chang PC, Sulik GI, Soong HK, Parkinson WC. Galvanotropic and galvanotaxic responses of corneal endothelial cells. J Formos Med Assoc 1996;95:623–627. [PubMed: 8870433]
19. Zhao M, Bai H, Wang E, Forrester JV, McCaig CD. Electrical stimulation directly induces pre-angiogenic responses in vascular endothelial cells by signaling through VEGF receptors. J Cell Sci 2004;117:397–405. [PubMed: 14679307]
20. Seghir T, Mahi D, Lebey T, Malec D. Analysis of the Electric Field and the Potential Distribution in Cavities Inside Solid Insulating Electrical Materials. The Proceedings of the COMSOL Users Conference at Paris. 2006
21. Lin F, Butcher EC. T cell chemotaxis in a simple microfluidic device. Lab Chip 2006;6:1462–1469. [PubMed: 17066171]
22. Unutmaz D, Xiang W, Sunshine MJ, Campbell J, Butcher E, Littman DR. The primate lentiviral receptor Bonzo/STRL33 is coordinately regulated with CCR5 and its expression pattern is conserved between human and mouse. J Immunol 2000;165:3284–3292. [PubMed: 10975845]
23. Lin F, Nguyen C, Wang S, Saadi W, Gross S, Jeon N. Neutrophil migration in opposing chemoattractant gradients using microfluidic chemotaxis devices. Ann Biomed Eng 2005;33:475–482. [PubMed: 15909653]
24. Lin F, Nguyen CM, Wang SJ, Saadi W, Gross SP, Jeon NL. Effective neutrophil chemotaxis is strongly influenced by mean IL-8 concentration. Biochem Biophys Res Commun 2004;319:576–581. [PubMed: 15178445]
25. Moghe PV, Nelson RD, Tranquillo RT. Cytokine-stimulated chemotaxis of human neutrophils in a 3-D conjoined fibrin gel assay. J Immunol Methods 1995;180:193–211. [PubMed: 7714334]
26. Foxman EF, Campbell JJ, Butcher EC. Multistep Navigation and the Combinatorial Control of Leukocyte Chemotaxis. J Cell Biol 1997;139:1349–1360. [PubMed: 9382879]
27. Foxman EF, Kunkel EJ, Butcher EC. Integrating Conflicting Chemotactic Signals: The Role of Memory in Leukocyte Navigation. J Cell Biol 1999;147:577–588. [PubMed: 10545501]
28. Chung CY, Funamoto S, Firtel RA. Signaling pathways controlling cell polarity and chemotaxis. Trends in Biochemical Sciences 2001;26:557–566. [PubMed: 11551793]
29. Sotsios Y, Whittaker GC, Westwick J, Ward SG. The CXC Chemokine Stromal Cell-Derived Factor Activates a Gi-Coupled Phosphoinositide 3-Kinase in T Lymphocytes. J Immunol 1999;163:5954–5963. [PubMed: 10570282]
30. Geissmann F, Cameron TO, Sidobre S, Manlongat N, Kronenberg M, Briskin MJ, Dustin ML, Littman DR. Intravascular Immune Surveillance by CXCR6+ NKT Cells Patrolling Liver Sinusoids. PLoS Biology 2005;3:e113. [PubMed: 15799695]

31. Hayday A, Tigelaar R. IMMUNOREGULATION IN THE TISSUES BY γδ T CELLS. NATURE REVIEWS IMMUNOLOGY 2003;3:233–242.

32. Shanley LJ, Walczysko P, Bain M, MacEwan DJ, Zhao M. Influx of extracellular Ca2+ is necessary for electrotaxis in Dictyostelium. J Cell Sci 2006;119:4741–4748. [PubMed: 17077123]

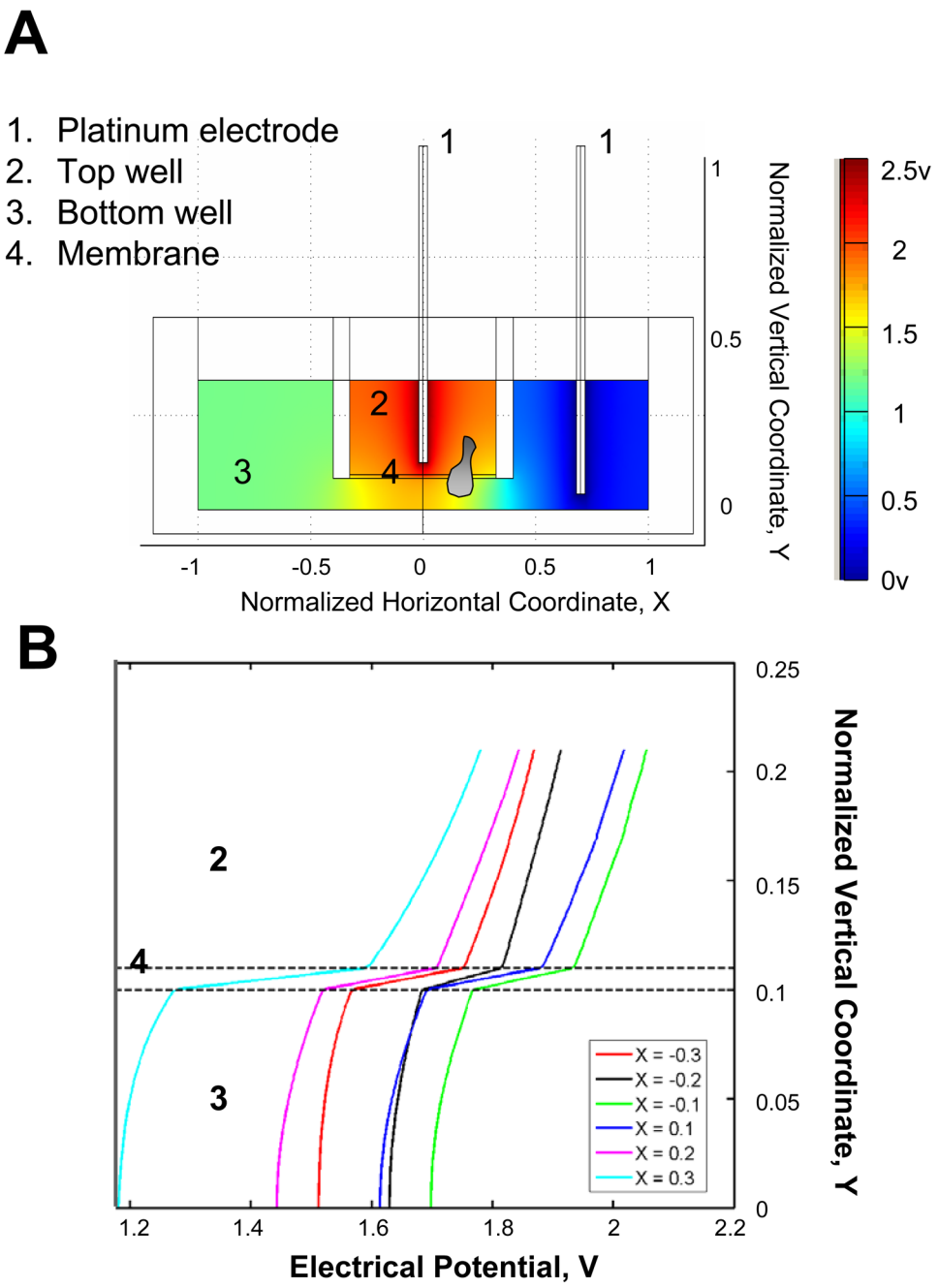

Figure 1. Transwell-based electrotaxis assay

(A) Illustration of transwell assay for studying cell migration in an applied electric field. An electric field was applied to the transwell (2.5V across the transwell) by placing two platinum electrodes, which were connected to a DC power supply, to the top and bottom well of the transwell respectively. Cells were allowed to migrate from the top well to the bottom well through the membrane. The electrical potential in the transwell assay was simulated. **(B)** The simulated electrical potential was plotted as a function of normalized vertical coordinate Y for different normalized horizontal coordinate X within the membrane (−0.3–0.3). 1 = 7.8mm for the normalized coordinate X. 1 = 10mm for the normalized coordinate Y.

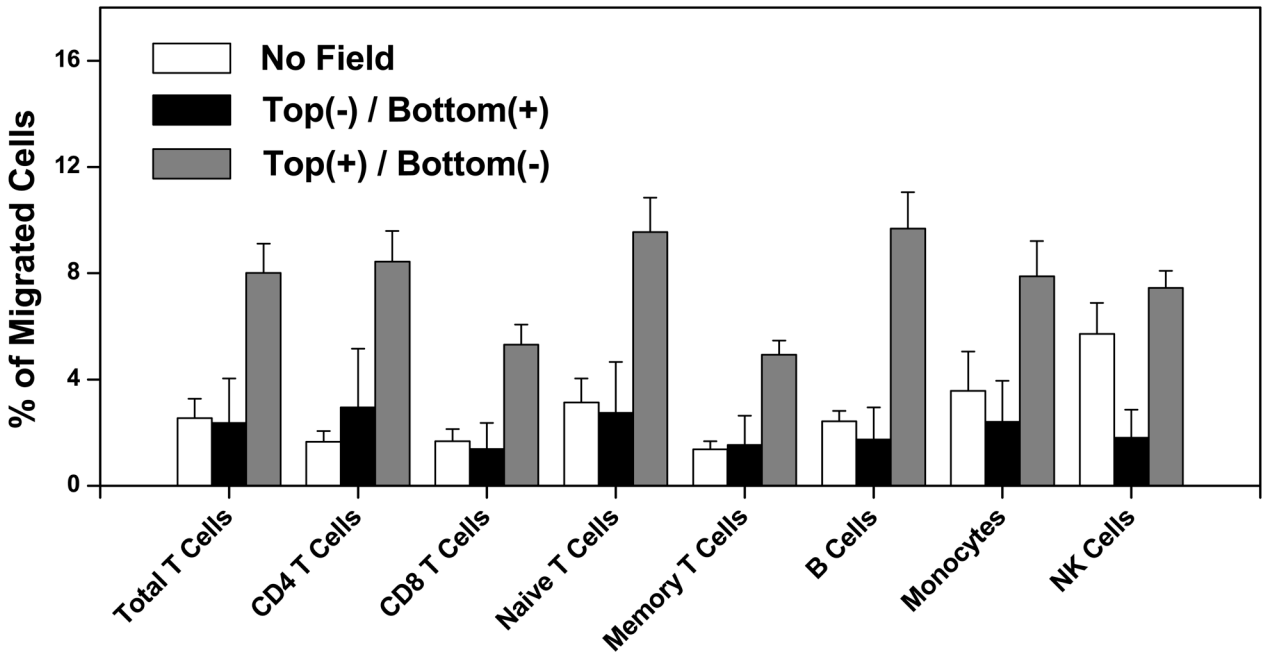

Figure 2. Migration of human blood lymphocytes and monocytes in an applied electric field

The migration of different subsets of hPBMC increased in transwell assay when the electric field was configured with the positive electrode in the upper well and the negative electrode in the bottom well (Top(+)/Bottom(−)) compared to it in the reversed electric field (Top(−)/Bottom(+)) or without the field. The error bars represent the standard error of the mean (s.e.m.) of multiple independent experiments (n = 9~11).

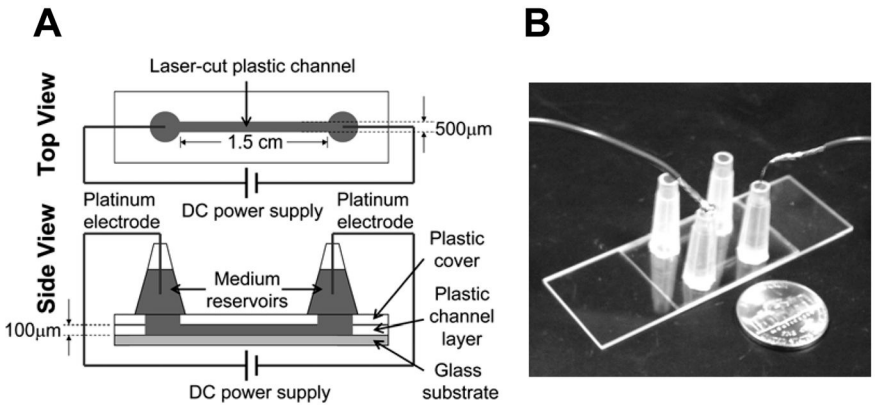

Figure 3. Microfluidic chamber for visualization of cell migration in an applied electric field

(A) Illustration of microfluidic system for studying cell migration in an applied electric field. **(B)** A picture of the microfluidic system. Two identical channels were configured side-by-side in a single device and can be used for migration studies separately. A nickle was placed next to the device as a scale reference.

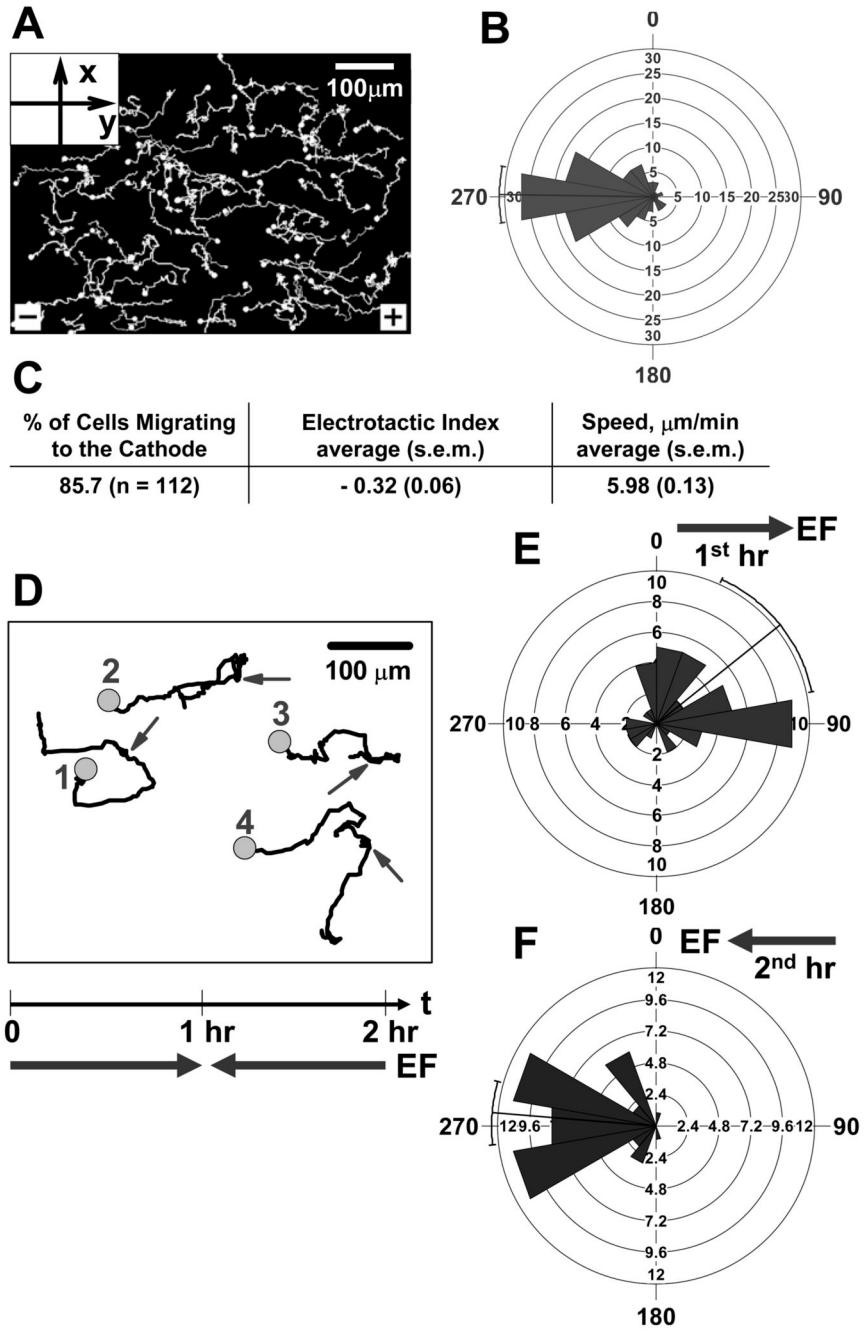

Figure 4. Directional migration of memory T cells in an applied electric field in vitro

(A) Cell tracks of a representative experiment show that cells preferentially migrate toward the cathode of the electric field (to the left, 270°). An electric field (1V cm^{-1}) was applied and the migration of cells was recorded for 30 min at 6 frames min^{-1}. The solid circles indicate the end of the tracks. **(B)** The rose diagram shows the distribution of migration angles (the migration angles were calculated from x-y coordinates at the beginning and the end of the cell tracks, and were grouped in 20° intervals, with the radius of each wedge indicating cell number). The mean angle vector and the 95% confidence interval were also shown. Rayleigh uniformity test confirmed that the distribution of migration angles is not uniform. The Modified Rayleigh test (V test) showed that the deviation of the migration angles from the direction of

electric field (270°) is not significant. **(C)** The percentage of cells migrated toward the cathode of the electric field, electrotactic index and the speed that were calculated using over 100 cell tracks from at least three independent experiments are presented in tabular form. Electrotactic Index and the speed are presented as the average value plus/minus the standard error of the mean (s.e.m.) of all cells. **(D–F)** Effects of field reversal. **(D)** Four representative cell tracks showing that cells migrated toward the cathode of the electric field and followed the reverse of the electric field (90° to 270° at the 60^{th} min). An electric field to the right (1V cm^{-1}) was applied for 1 hour and was reversed (to the left) for another hour. Migration of cells was recorded continuously for 2 hours at 6 frames min^{-1}. The circles indicate the end of the tracks and the arrows indicate when the electric field was reversed. Rose diagrams show the distribution of migration angles in the first hour **(E)** and the second hour **(F)** of the experiment (the migration angles were calculated from x-y coordinates at the beginning and the end of the cell tracks (n = 45), and were grouped in 20° intervals, with the radius of each wedge indicating cell number). The mean angle vector and the 95% confidence interval were also shown. Rayleigh uniformity test confirmed that the distribution of migration angles is not uniform. The Modified Rayleigh test (V test) showed that the deviations of the migration angles from the direction of electric field (90° in the first hour and 270° in the second hour) are not significant.

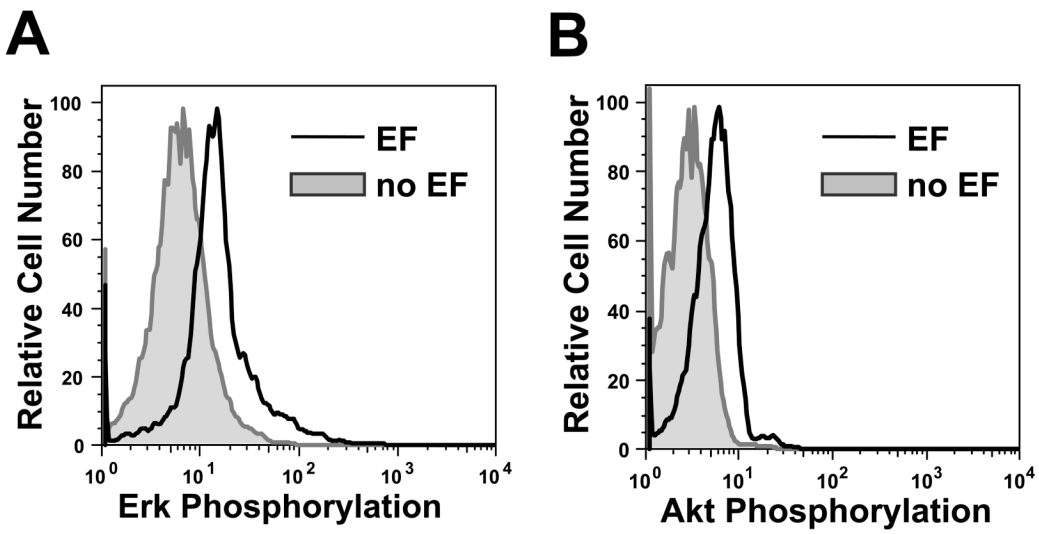

Figure 5. Signaling of human peripheral blood lymphocytes in an applied electric field

Phosphorylation of Erk1/2 **(A)** and Akt **(B)** is increased in an applied electric field as measured by phospho-flow cytometry. Cells were stimulated by an electric field (2.5V across ~1.3cm) for 60 min at room temperature in a 24-well plate. Stimulated cells, and unstimulated control cells incubated in parallel but without an electric field, were stained with anti-phospho-Erk1/2 antibody or anti-phospho-Akt-ser473 antibody. Each experiment was repeated at least 3 times with similar results

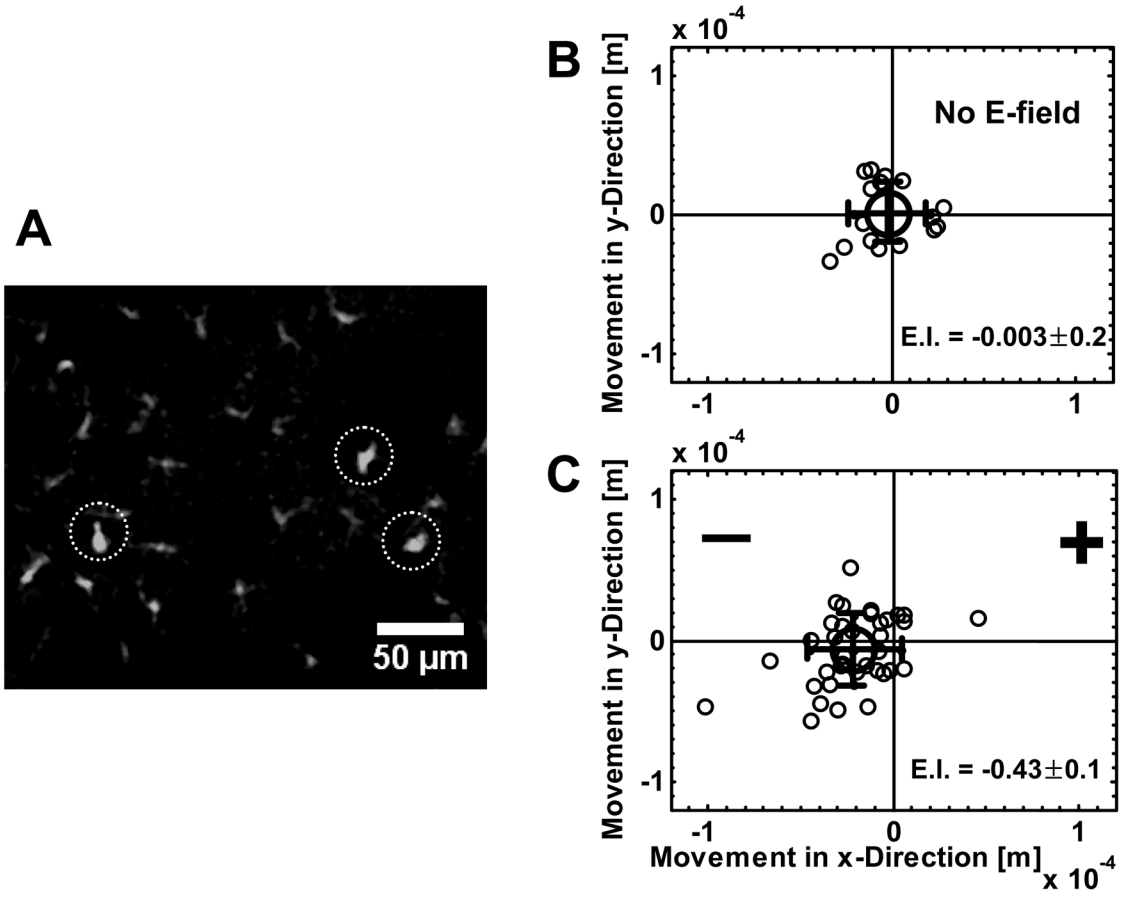

Figure 6. Migration of T cells in mouse ear pinna in response to an applied electric field

(A) Confocal image of CXCR6+ (GFP+) cells in the ear tissue of a CXCR6 GFP transgenic mouse (image selected from a single focal plane). The cells in circles are the migrating cells (these cells with lymphocytic morphology are motile and are typically outnumbered by sessile GFP+ cells of dendritic morphology in the ear tissue as visualized by confocal microscopy). **(B)** Distribution of motile lymphocytic cell displacement along the X and Y direction in the absence of an applied electric field. The large circle is the average cell displacement. The error bar represents standard deviation. **(C)** Distribution of motile lymphocytic cell displacement along the X and Y direction in an applied electric field (2.5V across ~5mm in the ear tissue). The large circle is the average cell displacement. The error bar represents standard deviation. Note that most cells were within the visible focal plane for only a fraction of the 1–2 hour visualization period. The electrostatic index (E.I.) is also shown as average ± s.e.m..